Electronic Supplementary Information

Synthesis of Open-mouthed, Yolk-Shell Au@AgPd Nanoparticles with Access to Interior Surfaces for Enhanced Electrocatalysis

Qiurong Shi, Peina Zhang, Yijing Li, Haibing Xia, Dayang Wang and Xutang Tao*

†State Key Laboratory of Crystal Materials, Shandong University, Jinan, 250100, P. R. China

‡Ian Wark Research Institute, University of South Australia, Adelaide, SA 5095, Australia

Experimental section

Materials

Chloroauric acid tetrahydrate ($HAuCl_4 \cdot 4H_2O$), trisodium citrate dihydrate ($Na_3C_6H_5O_7$) and ascorbic acid (AA) were purchased from Sinopharm Chemical Reagent Co. Ltd. Silver nitrate ($AgNO_3$, 99 +%), sodium tetrachloropalladate (II) (Na_2PdCl_4, 99 %), and hydroquinone (HQ, 99 %) was purchased from Alfa Aesar (Tianjin, China). All glasswares and stirring bars were cleaned with aqua regia (3:1 v/v HCl (37 %): HNO_3 (65 %) solutions) and then rinsed thoroughly with H_2O before use. (*Caution: aqua regia solutions are dangerous and should be used with extreme care; never store these solutions in closed containers.*) The water in all experiments was prepared in a three-stage Millipore Milli-Q plus 185 purification system and had a resistivity higher than 18.2 MΩ cm.

Synthesis of 30 nm Au NPs by our premixing method

Gold nanoparticles (Au NPs) with sizes of 30 nm as seeds were synthesized via our premixing method reported elsewhere.[1] Typically, 0.65 mL of aqueous citrate solution (1 wt %) were added to 1.1 mL of water, followed by adding 0.75 mL of aqueous $HAuCl_4$ solution (1 wt %) and 42.5 μL of aqueous $AgNO_3$ solution (0.1 wt %) successively. After incubation of about 4.5 min, this premixture was quickly poured into 47.5 mL of boiling water in a 100 mL flask. Further reflux of the whole reaction solution was continued for 1 h under stirring to warrant the formation of uniform quasi-spherical Au NPs.

Synthesis of core-shell Au@Ag NPs with Ag shell of different thicknesses (denoted as CS_n Au@Ag NPs, in which n is the thickness of the shell)

A typical synthesis of $CS_{5.4}$ Au@Ag NPs with 30 nm Au core is as fellows. 300 μL of aqueous citrate solution (1 wt %) were added into 8.650 mL of water, followed by adding 1 mL of aqueous solution of as-prepared 30 nm Au NPs, 20 μL of aqueous HQ solution (0.03 M) and 30 μL of aqueous $AgNO_3$ solution (0.01 M) successively. After about stirring of 4 h, the color of the aqueous solution was changed from light red to orange. Eventually, core-shell Au@Ag NPs with 5.4 nm Ag shell were obtained. The detailed synthetic conditions for core-shell Au@Ag NPs with Ag shell of other thickness were as follows.The detailed synthetic conditions for core-shell Au@Ag NPs with Ag shell of other thickness were as follows (Table S1).

Synthesis of open-mouthed, yolk-shell Au@AgPd NPs (OM-YS Au@AgPd NPs).

The OM-YS Au@AgPd NPs were fabricated via galvanic replacement reactions of Ag shells of Au@Ag NPs with Pd^{2+} ions at room temperature. Typically, 150 μL of aqueousNa_2PdCl_4 solution (1 mM) were immediately added into 10 mL of aqueous solution of as-obtained $CS_{5.4}$ Au@Ag NPs. The reaction was further stirred for about 4 h at room temperature. The color of the aqueous solution changed from orange to grayish pink. The product was centrifuged at 8000 rcf for 10 min, and then washed 2 times more with Milli-Q water.

Synthesis of core-shell Au@AgPd NPs, half-encased, core-shell Au@AgPd NPs and conventional yolk-shell Au@Pd NPs

The whole synthetic procedure is nearly same except that the atomic ratio of Pd to Ag was adjusted according to the Ag shell thickness of Au@Ag NPs used (see Table S2 for details).

The core-shell Au@AgPd NPs were fabricated by adding 20 μL of aqueous Na_2PdCl_4 solution (1 mM) into 10 mL of aqueous solution of $CS_{1.8}$ Au@Ag NPs obtained. The reactions were further stirred for about 4 h at room temperature. The color of the aqueous solution changed from yellowish pink to light pink. The products were centrifuged at 8000 rcf for 10 min and washed in turn 2 times with de-ionized water.

The half-encased, CS Au@AgPd NPs were fabricated by adding 20 μL of aqueous Na_2PdCl_4 solution (1 mM) into the 10 mL of aqueous solution of $CS_{5.4}$ Au@Ag NPs obtained. The reactions were further stirred for about 4 h at room temperature. The color of the aqueous solution changed from orange to light grayish pink. The products were centrifuged at 8000 rcf for 10 min and washed in turn 2 times with de-ionized water.

The conventional yolk-shell Au@AgPd NPs were fabricated by adding 40 μL of aqueous Na_2PdCl_4 solution (10 mM) into 10 mL of aqueous solution of $CS_{6.3}$ Au@Ag NPs obtained. The reactions were further stirred for about 4 h at room temperature. The color of the aqueous solution changed from orange to brown. The products were centrifuged at 8000 rcf for 10 min and washed in turn 2 times with de-ionized water.

Synthesis of hollow AgPd NPs

Ag NPs were firstly prepared via our previous method,[2] 50 μL of the aqueous solution of AA with the concentration of 0.10 M was added into 47.5 mL of boiling water, followed by boiling for an additional 1 min. 1 mL of the aqueous solution of sodium citrate (1 wt %) and 0.25 mL of the aqueous solution of $AgNO_3$ (1 wt %) were consecutively added to 1.25 mL of water under stirring at room temperature. After 5 min incubation at room temperature, the mixture solution was injected into the boiling aqueous solutions of AA (just after 1 min

boiling after AA addition to boiling water). The color of the reaction solution quickly changed from colorless to yellow.

Hollow AgPd NPs were synthesized via galvanic displacement reaction. Typically, 2.5 mL aqueous solution of Na_2PdCl_4 (0.25 mM) was injected to 5 mL of the aqueous solution of as-prepared Ag NCs at a rate of 100 μL /min. The solution was under vigorous stirring for about 4 hours at room temperature. The color was changed from transparent yellow to dark yellow and finally become dark brown.

Synthesis of hollow AgPd NPs with open mouths

The solution of as-prepared hollow AgPd NPs (7.5 mL) were treated by H_2O_2 (60 μL, 0.3 wt%) to remove excess Ag. Eventually, hollow AgPd NPs with open mouths were obtained by centrifugation (13000 rcf, 15 min).

Synthesis of core-shell Au@Pd NPs

300 μL of aqueous citrate solution (1 wt %) were added into 8.650 mL of water, followed by adding 1 mL of aqueous solution of as-prepared 30 nm Au NPs, 80μL of aqueous Na_2PdCl_2 solution (0.01 M) and 100 μL of aqueous AA solution (0.1 M) successively. After about stirring of 4 h, core-shell Au@Pd NPs with about 4 nm Pd shell were obtained.

CO-stripping experiments

The CO stripping voltammetry was performed in 0.3 M KOH solution at room temperature. After purging the solution with ultrapure N_2 for 30 min, ultrapure CO gas was bubbled for 20 min under a fixed potential of -0.3 V vs Ag/AgCl, to promote the formation of a CO adlayer on the surface of the catalyst. Further, dissolved CO was flushed out by purging the solution with ultrapure N_2 for 30 min The CO stripping voltammetry patterns were recorded at a potential scan rate of 50 mV s^{-1}.

Characterization

Cyclic voltammetric (CV) and chronoamperomeric (CA) experiments were performed in a standard three-electrode cell in a CHI660D workstation at room temperature.

A glassy carbon electrode (GCE) modified by as-prepared Au@AgPd NPs employed as the working electrode while an Ag/AgCl electrode and Pt wire were used as the reference electrode and auxiliary electrode, respectively. The bare GCE was polished with 300 and 50 nm alumina slurry successively, followed by rinsing thoroughly with pure water and drying at room temperature.

Preparation of glassy carbon electrode (GCE) with Pd/C catalysts. Typically, 11.2 mg of

commercial Pd/C catalyst (5 % on activated carbon powder, eggshell, reduced, nominally 50 % water wet) was dispersed in 1 mL of H_2O by continual ultrasonic for 5 min. 6 μL of commercial Pd/C solution was drop-coated on the bare glassy carbon electrode (GCE), followed by drying in air. 10 μL of the ethanol solution of Nafion (0.2 wt %) was then cast on the surface of the GCE electrodes coated by commercial Pd/C catalyst, followed by drying in air for further use.

Preparation of glassy carbon electrode (GCE) with Au@AgPd NPs.16 μL of Au@AgPd NP solution after centrifugation was drop-coated on the prepared bare GCE, followed by drying in air. 10 μL of the ethanol solution of Nafion (0.2 wt %) was then cast on the surface of the GCE electrodes coated by Au@AgPd NPs, followed by drying in air for further use.

Cyclic voltammograms of the resulting Au@AgPd NPs were recorded in 0.30 M KOH and 0.50 M ethanol, while the solutions were purged with high purity nitrogen (99.99 %) for 30 min prior to the test.

Figure S1. TEM images of as-prepared 30 nm Au NPs obtained via the Ag(I)-assisted reduction of $HAuCl_4$ with citrate in boiling water (a) and CS_n Au@Ag NPs with different thickness of Ag shell (b-f) by adjusting different amounts of silver nitrate as well as hydroquinone (HQ): 0.10 μmol (b), 0.20 μmol (c), 0.35 μmol (e), 0.50 μmol (e) and 0.70 μmol (f). The molar ratio of $AgNO_3$ to HQ is kept as about 2. The insets in the TEM images (a-f) are the corresponding sample photos.

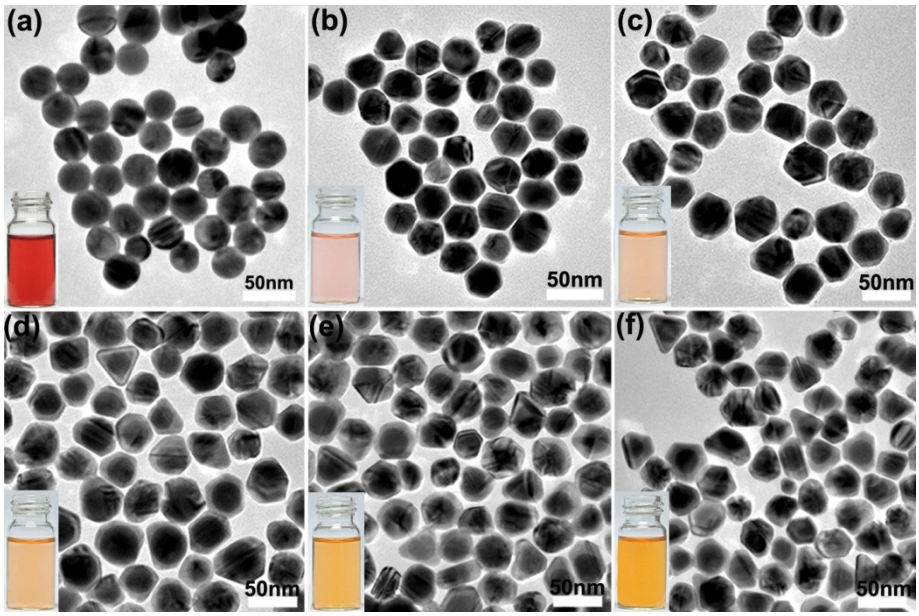

Monodisperse, quasi-spherical Au NPs with average diameter of 30 nm were prepared via the Ag(I)-assisted reduction of $HAuCl_4$ with citrate in boiling water.[1] These Au NPs have a narrow size distribution and exhibit nearly quasi-spherical shape (Figure S1a).The CS Au@Ag NPs were prepared by hydroquinone (HQ) reduction of $AgNO_3$ on the surfaces of as-prepared Au NPs as seeds in water at room temperature. A series of experiments were conducted to prepare CS Au@Ag NPs with Ag shell of different thickness by adjusting the amount of silver as well as HQ (Figure S1b-1f and Table S1).

Figure S2. UV-vis spectra (a to f) of as-prepared 30 nm Au NPs (a, black curve) and CS_n Au@Ag NPs with different thickness of Ag shell (b to f) by adjusting different amounts of $AgNO_3$ as well as hydroquinone (HQ): 0.10 μmol (b, red curve), 0.20 μmol (c, blue curve), 0.35 μmol (d, dark cyan), 0.50 μmol (e, magenta) and 0.70 μmol (f, green).

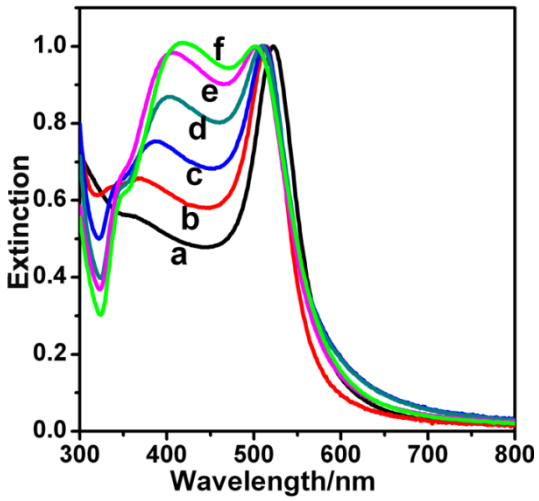

The UV-vis spectrum of Au NPs has a rather symmetric surface plasmon resonance band and no nonzero extinction baseline at longer wavelength (black curve, Figure S2a), underlining the good quality of Au NPs obtained. The Au NPs show the absorption peak centered at about 521 nm, characteristic of quasi-spherical Au NPs. Accordingly, the Ag shell of different thickness could also be inferred from UV-vis spectra (Figure S2b to S2f, and Table S3). The SPR peak positions of Au cores are blue-shifted from 514 nm to 501 nm and the Ag shells are red-shifted from 361 nm to 420 nm in UV-vis spectra (Figure S2 and Table S3) when the thickness of Ag shells are increased from 1.8 nm to 7.6 nm (Figure S1b to S1f and Table S1), respectively.

Figure S3. TEM images (a and b) of the as-prepared $CS_{1.8}$ Au@Ag NPs (a), the obtained CS Au@AgPd NPs via adding Pd^{2+} into the aqueous $CS_{1.8}$ Au@Ag solution (b) and UV-vis spectra (c) of $CS_{1.8}$ Au@Ag NPs (a, black curve) and CS Au@AgPd NPs (b, red curve).

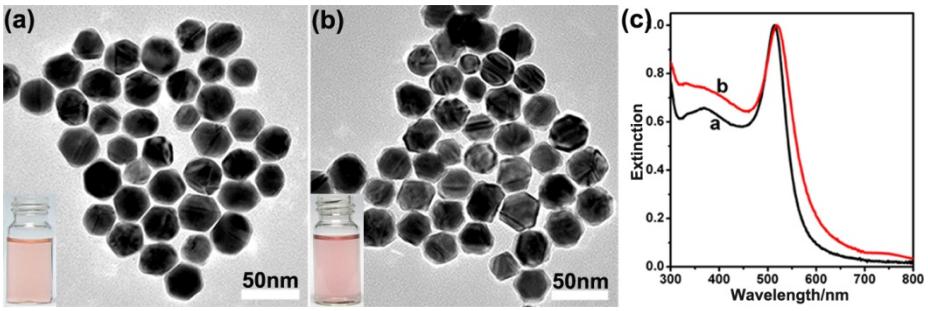

In general, galvanic displacement happens between two metals with electric potential difference. The reaction between Ag and Pd^{2+} ions in our case is as follows:

$$PdCl_4^{2-} + 2\,Ag = Pd + 2\,Ag^+ + 4\,Cl^- \qquad (1)$$

It can be seen that two Ag atoms can be replaced by one Pd^{2+} ion in this reaction. For CS Au@Ag NPs with an initial Ag shell thickness of less than 3 nm (Figure S3a), yolk-shell structure cannot form when the molar ratio of Pd^{2+} ions to Ag atoms was changed from 0 to 1 (Table S2). These $CS_{1.8}$ Au@Ag NPs were simply evolved to CS Au@AgPd NPs (Figure S3b). The $CS_{1.8}$ Au@Ag NPs obtained shows two SPR peaks, which are centered at about 514 nm for cores of Au NPs and 361 nm for Ag shells, respectively. The disappearance of the peak centered at about 361 nm and appearance of the broad peak indicate the formation of Pd/Ag shell after galvanic exchange reaction with Pd^{2+} ions; the peak position of the cores of Au NPs is also slightly red shifted from 514 nm to 518 nm due to the formation of Pd/Ag shell (red curve in Figure S3c).

Figure S4.TEM images of the as-prepared $CS_{5.4}$ Au@Ag NPs (a), the half-encased CS Au@AgPd NPs obtained (b) and OM-YS Au@AgPd NPs (c) via adding Pd^{2+} ions of different amount into the aqueous solution of $CS_{5.4}$ Au@Ag NPs, respectively. (d) UV-vis spectra of $CS_{5.4}$ Au@Ag NPs (a, black curve), half-encased CS Au@AgPd NPs (b, red curve) and OM-YS Au@AgPd NPs (c, blue curve).

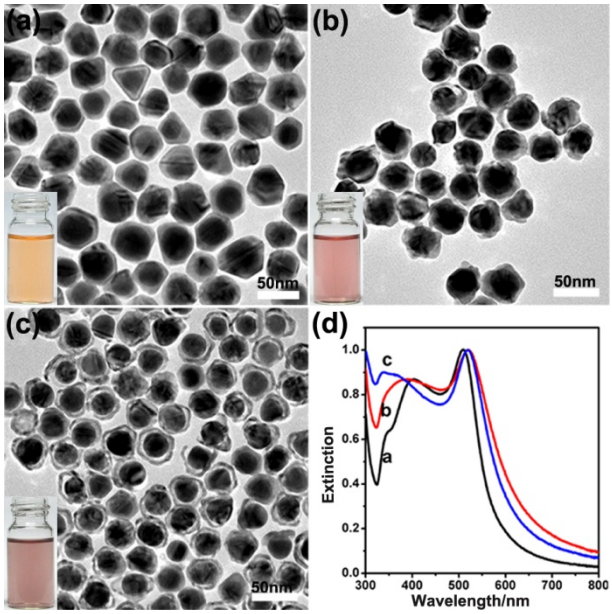

For CS Au@Ag NPs with an initial Ag shell thickness between 3 nm and 6 nm (Figure S4a), Au@AgPd NPs of different structures were obtained under different molar ratios of Pd^{2+} ions to Ag atoms. When the molar ratio of Pd^{2+} ions to Ag atoms was below 0.2, NPs composed of Au cores and half-encased, thicker Pd/Ag shells were obtained (Figure S4b). When the molar ratio of Pd^{2+} ions to Ag atoms was between 0.2 and 0.5, the OM-YS Au@AgPd NPs started to appear, companied with half-encased CS Au@AgPd NPs. When the molar ratio of Pd^{2+} ions to Ag atoms reached 0.5, the OM-YS Au@AgPd NPs were obtained. When the molar ratio of Pd^{2+} ions to Ag atoms was between 0.5 and 1, the same OM-YS Au@AgPd NPs were still obtained except the slight increase in thickness of Pd shell. The peak position of half-encased CS Au@AgPd NPs and OM-YS Au@AgPd NPs both show blue-shift from 403 nm to 360 nm and 340 nm, respectively, compared to that of $CS_{5.4}$ Au@Ag NPs at 403 nm, demonstrating that Ag shells were replaced by Pd shells.

Figure S5. TEM images of the as-prepared $CS_{6.3}$ Au@Ag NPs (a), the obtained half-encased CS Au@AgPd NPs (b), and conventional YS Au@AgPd NPs (c) via adding Pd^{2+} ions into the aqueous solution of $CS_{6.3}$ Au@Ag NPs, respectively. (d) UV-vis spectra of $CS_{6.3}$ Au@Ag NPs (a, black curve), half-encased CS Au@AgPd NPs (b, red curve) and conventional YS Au@AgPd NPs (c, blue curve).

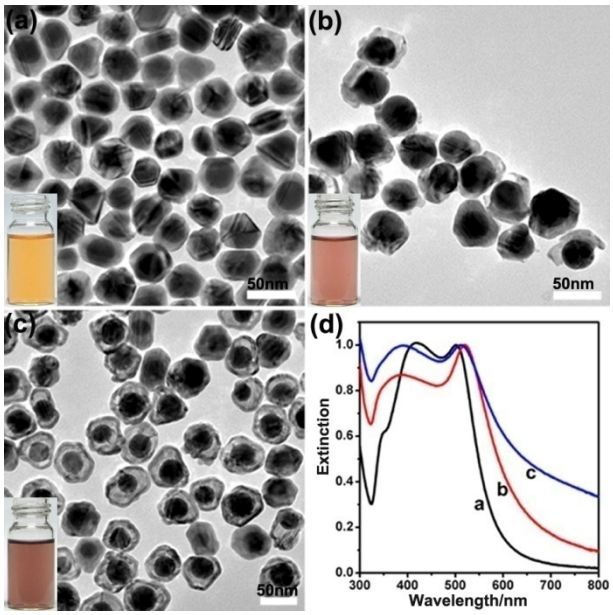

For CS Au@Ag NPs with an initial Ag shell thickness of more than 6 nm (Figure S5a), Au@AgPd NPs of different structures were also obtained under different molar ratios of Pd^{2+} ions to Ag atoms. When the molar ratio of Pd^{2+} ions to Ag atoms was below 0.3, NPs composed of Au cores and half-encased, thicker Pd/Ag shells were obtained (Figure S5b). When the molar ratio of Pd^{2+} ions to Ag atoms was between0.3 and 1, the conventional YS Au@AgPd NPs with intact Pd shells (Figure S5c) in high yield were obtained. The peak positions of half-encased CS Au@AgPd NPs and conventional YS Au@AgPd NPs were both around 380 nm; their intensity was increased with the amount of Pd^{2+} ions used.

Possible formation mechanism of core-shell Au@AgPd NPs, half-encased, core-shell Au@AgPd NPs, conventional yolk-shell Au@AgPd NPs and open-mouthed, yolk-shell Au@AgPd NPs

Diffusion processes are enhanced in nanocrystals[3-5] due to the following factors: (i) the large volume fraction of the interfaces formed in these structures, which provides short-circuit diffusion paths; (ii) a high density of defects, such as grain boundaries and vacancies caused by the galvanic replacement; (iii) existence of driving forces, for example, stress fields and dislocations in the crystals that may introduce fast diffusion paths;[6] and (iv)defects originating from the curvature of surfaces. In our cases, gold and silver have the same face-centered cubic (fcc) structure and about equal lattice constants. Therefore, Ag atoms are epitaxially deposited onto the Au surface at initial stage and the growth characteristic of Ag dominates after its thickness exceeding the critical value at later stage. Consequently, the surfaces of thicker Ag shells are rougher than those of thinner ones and have a higher density of defects. It is known that for single-component metal NPs, the electrochemical potential required for dissolution of the metal species is greatly affected by the curvature of the surface due to a Gibbs−Thomson effect.[7,8] At a fixed potential, the surface of a NP is quickly passivated by the layer of more-noble component as the less-noble metal is etched from defect sites on the NP's surface. After some time, a NP with rough surfaces may lead to the existence of more uncovered areas among the passivation layer than that with smooth surface. In other words, for Au@Ag NPs with thicker Ag shells (say between 3 nm and 6 nm in our case), their surfacespossess more defect sites. Accordingly, more uncovered areas are present on the surfaces of Au@Ag NPs as Ag is easily etched at defect sites and Pd shells are formed at sites with fewer defects. However, after generation of a pit on defect site of the surface, the pit acts as an active site where exposed Ag atom is readily oxidized to Ag^+ ion. Further replacement occurs only at the pit and causes expansion of the hole, yielding a single open-mouthed structure without damaging the remaining silver regions.[9]Another possible factor is due to short-circuit diffusion path,[2]in which the effective electron transfer from the hole to the NP surface. The electrons generated from the oxidation of Ag atoms to Ag^+ ions at the pit are transferred to the rod surface through conductive media (Ag and Pd domains); the Pd^{2+}ions in solution are then reduced to Pd atoms and evenly deposited on the surface.[9]For Au@Ag NPs with thinner Ag shells (say below 3 nm in our case), their surfaces possess fewer defect sites, thus leaving fewer uncovered areas after formation of Pd layer and further leading to stop of Ag dissolution. Therefore, core-shell Au@AgPd

NPs were easily obtained (Figure S3). For Au@Ag with thicker Ag shell (say above 6 nm in our case), more defect sites are present on their surface. In addition, the concentration of Pd^{2+} ions used is much higher at the same molar ratio of Pd^{2+} ions to Ag atoms due to increasing Ag shell. Therefore, fast formation of Pd layer on the sites with less defect and subsequent fast growth lead to formation of conventional YS Au@AgPd NPs (Figure S5c). When the thickness of Ag shells on core-shell Au@Ag NPs and molar ratio of Pd^{2+} to Ag (about equal to 0.5) both are under optimal conditions, the striking OM-YS Au@AgPd NPs can be synthesized in high yield (Figure S4c).

Figure S6. XRD pattern of as-preparedOM-YS Au@AgPd NPs.

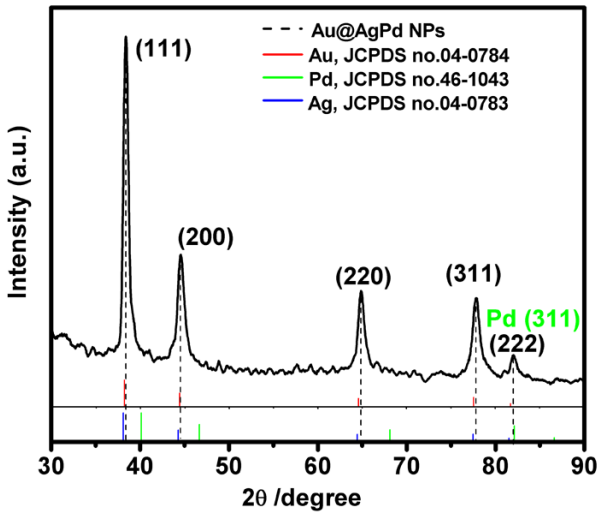

Figure S7. Low magnification SEM image of OM-YS Au@AgPd NPs. OM-YS Au@AgPd NPs are derived from CS NPs with 30 nm Au NPs and 5.4 nm thick Ag shells via galvanic reactions at room temperature. The Pd^{2+} to Ag molar ratio is 0.5 and the citrate concentration is 0.03 wt%.

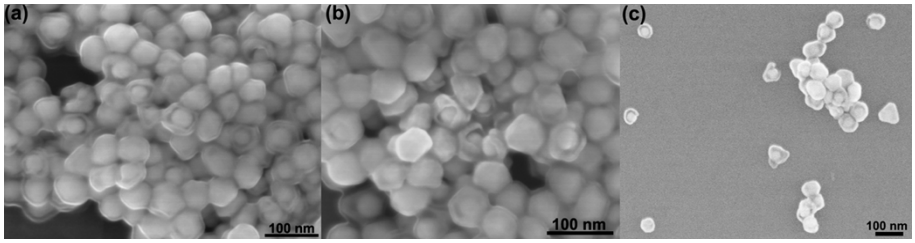

Due to random agglomeration of YS Au@AgPd NPs on the substrates, not all of open mouths on YS Au@AgPd NPs can directly show up (Figure S7). In addition, the samples cannot be easily titled by the SEM. Thus, a set of TEM images of as-preparedOM-YS Au@AgPd NPs are recorded at different tilting angles, -20° and 0° with respect to the axis of rotation (Fig. 2c and 2d). Furthermore, TEM three-dimensional (3D) tomography of a single OM-YS Au@AgPd NP was also implemented by imaging the NP at different specimen orientations.

Figure S8.HAADF-STEM-EDS mapping images (a to d) and cross-sectional compositional line profiles (e) of the conventional YS $Au_{0.42}@Ag_{0.33}Pd_{0.25}$ NPs. The inset in Figure S8e is the HAADF-STEM image of the conventional YS $Au_{0.42}@Ag_{0.33}Pd_{0.25}$ NPs.

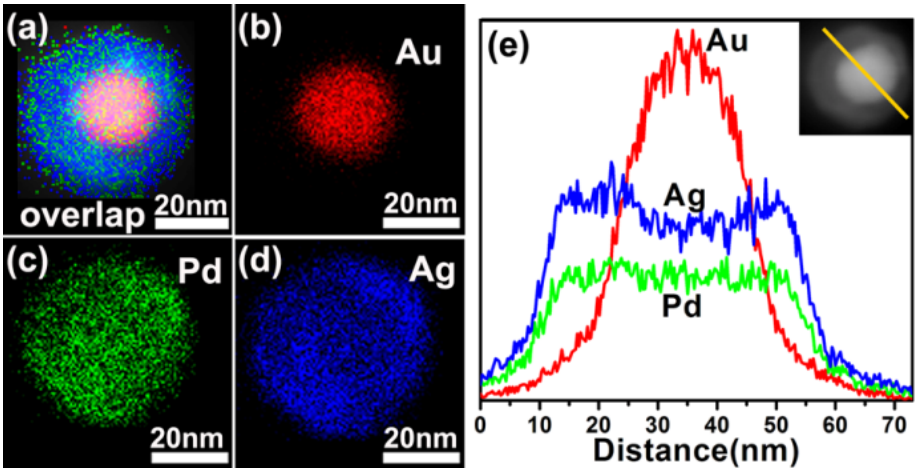

The HAADF-STEM-EDS mapping images of the conventional YS $Au_{0.42}@Ag_{0.33}Pd_{0.25}$ NPs (Figure S8a to S8d) show that each element (Au, Pd and Ag) exhibits spherical shape; there is no open-mouth in the overlapped image. In addition, the difference in the element composition and structure of the OM-YS Au@AgPd NP and the conventional YS Au@AgPd NPs was further confirmed by cross-sectional compositional line profiles (Figure 4eand S8e).

Figure S9. UV-vis spectra of conventional (a) and open-mouthed (b) YS Au@AgPd NPs obtained in different solvents of varying refractive indexes.

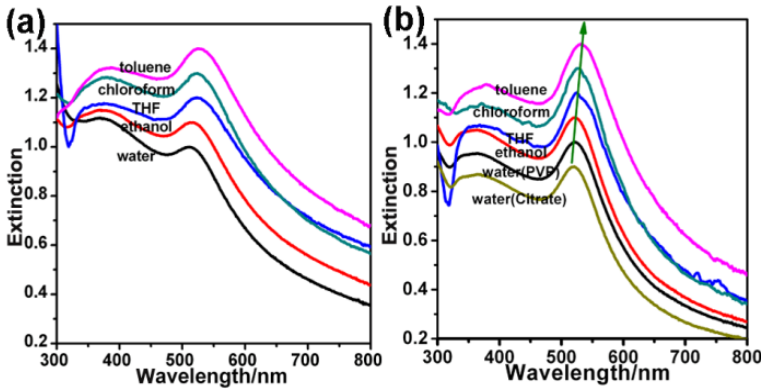

The samples (conventional and open-mouthed, YS Au@AgPd NPs) stabilized by citrate cannot be directly dispersed into organic solvents as they will aggregate and precipitate finally. Therefore, these NPs are stabilized by PVP polymer by ligand exchange. In their UV-vis spectra, the peak positions of Au cores in conventional and open-mouthed, YS Au@AgPd NPs samples in water stabilized by PVP are still kept as at about 519 nm and 511 nm, respectively, which are same with those stabilized by citrate. The results indicate that the substitution of citrate by PVP ligand has no effect on the UV-vis spectra of our samples in water. The NPs stabilized by PVP polymer can disperse in water and ethanol. However, they are still easily aggregated in other organic solvents (i.e. THF, chloroform, and toluene). Therefore, a series of mixed solvent were prepared according to the volume ratio of ethanol to other organic solvents as 1:9. Accordingly, the effective refractive index (n_{eff}) is revised by the following equation (Table S4):

$$n_{eff(THF/chloroform/toluene)} = 0.9 * n_{eff(THF/chloroform/toluene)} + 0.1 * n_{ethanol} \quad (2)$$

Figure S10.CV curves of the GCEs modified by OM-YS Au@AgPd NPs (a, black curve), YS Au@AgPd NPs (b, red curve) and commercial Pd/C catalyst (c, blue curve), respectively, in 0.30 M N_2-saturated KOH aqueous solution at room temperature. The currentsshown in the Figure are normalized by the Pd mass loaded. The scan ratesare 50 mVs^{-1}.

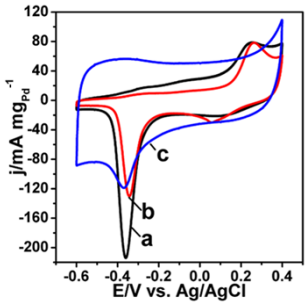

Figure S11.CV curves (A and B) and potential cycling stability (C) of the GCE modified by OM-YS Au@AgPd NPs with a negligible amount of Ag (a, black curve) prepared from $CS_{5.4}$ Au@Ag NPsand a noticeable amount of Ag (b, magenta curve) on the surfaces prepared from $CS_{3.6}$ Au@Ag NPs in 0.3 M N_2-saturated KOH aqueous solution in the absence (A) and presence of 0.5 M ethanol (B, C and D) at room temperature. The scan rate of (A) and (B and C) was 50 mV s^{-1} and 20 mV s^{-1}, respectively. The current in (A and B) and (C) was normalized by the Pd mass loaded on GCE and the ECSA values, respectively.

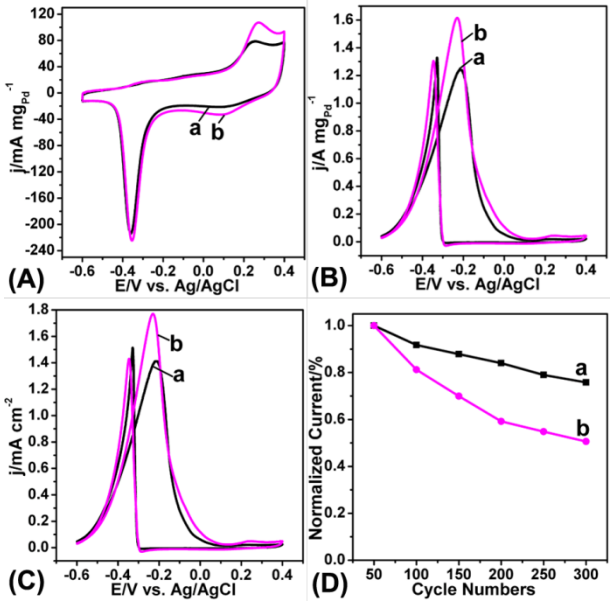

Figure S12. TEM image of conventional YS Au@AgPd NPs after durability test.

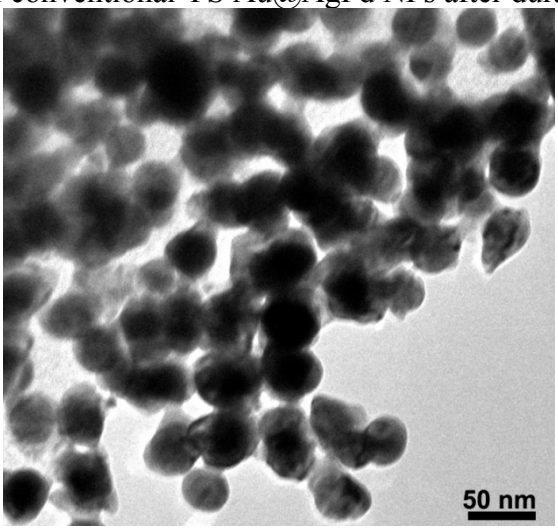

Figure S13. TEM images of OM-YS Au@AgPd NPs after durability test.

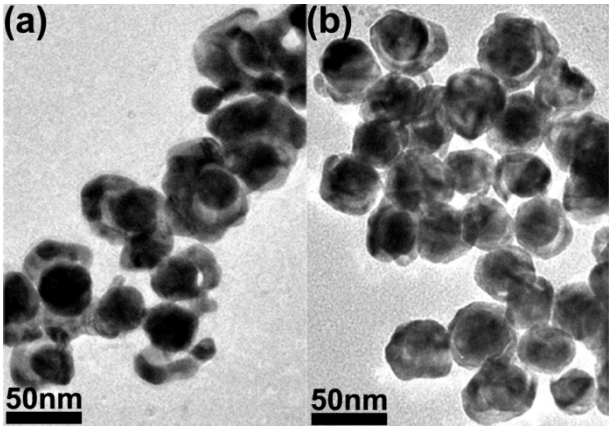

Figure S14. (a) TEM images of CS $Au_{0.83}@Pd_{0.17}$ NPs and (b) hollow $Ag_{0.78}Pd_{0.22}$ NPs.

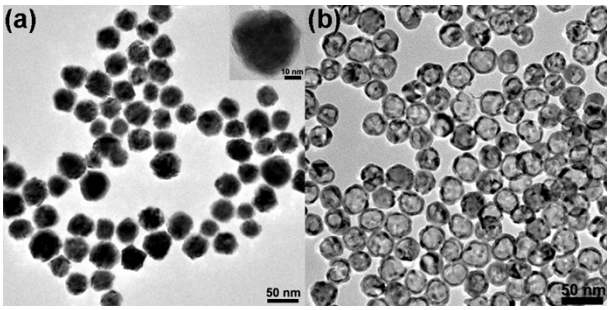

The main purpose of the synthesis of CS Au@Pd NPs was used to demonstrate that pure Pd shells are still easily poisoned, in comparison with our samples.

Figure S15. (A) TEM image of hollow AgPd NPs with open mouths, (B) TEM images of a hollow AgPd NP with open mouths taken at different tilting angles from 45°(a) to -45° (g) with respect to the rotation axis. (C) TEM image of hollow AgPd NPs with open mouths after stability test.

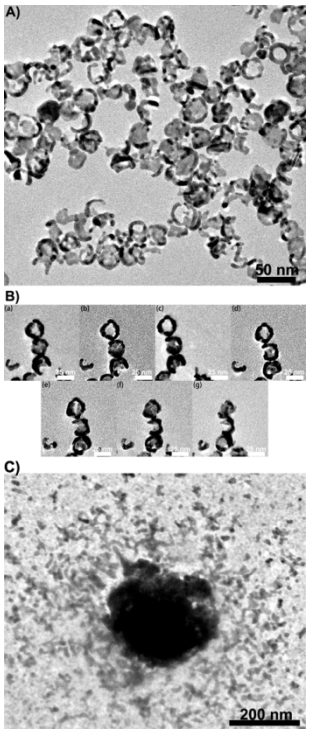

Figure S16.CV curves of the GCEs modified by hollow $Ag_{0.73}Pd_{0.27}$ NPs with open mouths (a, black curve), hollow $Ag_{0.78}Pd_{0.22}$ NPs (b, red curve) and CS $Au_{0.83}@Pd_{0.17}$ NPs (c, blue curve), respectively, in 0.30 M N_2-saturated KOH aqueous solution at room temperature. The currentsshown in the Figure are normalized by the Pd mass loaded. The scan ratesare 50 mVs^{-1}.

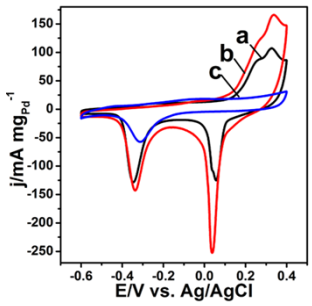

Figure S17.CV curves (A), chronoamperomeric curves (B) and potential cycling stability (C) of the GCEs modified by hollow $Ag_{0.73}Pd_{0.27}$ NPs with open mouths (a, black curve), hollow $Ag_{0.78}Pd_{0.22}$ NPs (b, red curve) and CS $Au_{0.83}@Pd_{0.17}$ NPs (c, blue curve) in 0.30 M N_2-saturated KOH aqueous solution at room temperature in the presence of 0.50 M ethanol. The currentsshown in Figure A and Bare normalized by the Pd mass loaded. The chronoamperomeric curves (B) are recorded at -0.3 V. The scan rates of (A) and (C) are 20 mV s^{-1} and 50 mV s^{-1}, respectively.

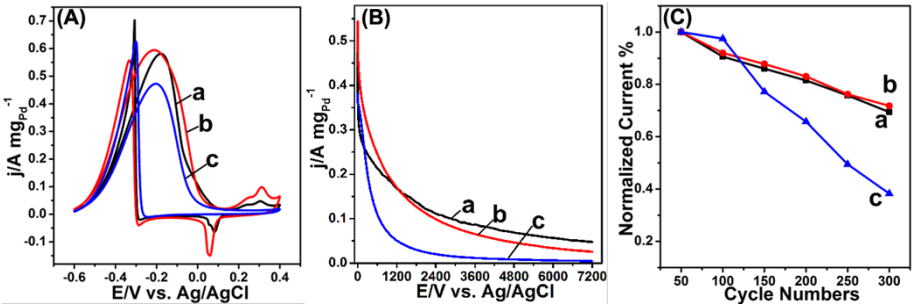

Figure S18. CO stripping measurements of Ag NPs (a), Au NPs (b),OMhollowAgPd NPs(c) and hollow AgPd NPs (d), performed in solution of 1.0 M KOH at 50 mV s^{-1}.

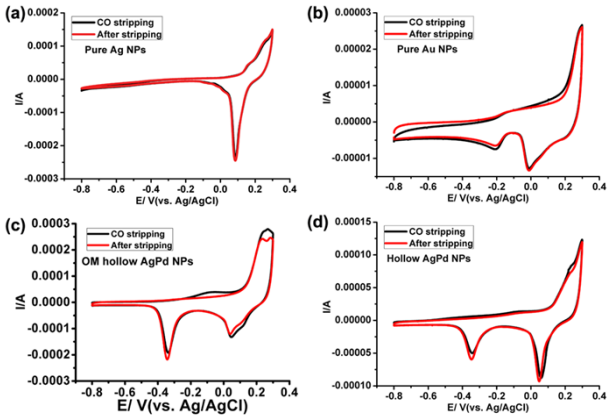

Pure Ag shows no peak associated with CO oxidation (Figure S18a). Pure Au also shows no peak associated with CO oxidation (Figure S18b) except one prewave connected with partial charge transfer to adsorbed OH^- anions.[10,11]The CVs of OM hollow AgPd NPs and hollow AgPd NPs without holes both show tiny peaks associated with CO oxidation due to formation of Pd–Ag alloy on the surfaces (Figures S18c and S18d). In these CVs, the presence of obvious CO oxidation peak is due to the decrease of the amount of Ag on the shell surfaces (Figures7c, S18c,7d and S18d). Although higher ratio of Ag on the AgPd shells can prohibit the CO adsorption at the initial stage, the exposed Pd shell are easily poisoned after Ag dissolution at later stage,which was demonstrated by the stability of conventional YS Au@AgPd NPs (Figure S12).

Table S1. Summary of synthetic conditions for CS_n Au@Ag NPs via tuning the amount of $AgNO_3$ (0.01 M) as well as HQ (0.03 M) at the fixed citrate concentration (1 wt %) and fixed amount of as-prepared Au NPs with sizes of 30 nm as cores.

H_2O (ml)	Citrate (μL)	Au NPs (mL)	HQ (μL)	$AgNO_3$ (μL)	Thickness of Ag shell (nm)
8.7	300	1.0	10	10	1.8±0.2
8.7	300	1.0	10	20	3.6±0.3
8.6	300	1.0	20	30	5.4±0.2
8.6	300	1.0	25	50	6.3±0.3
8.6	300	1.0	70	70	7.6±0.5

Table S2. Summary of Au@AgPd NPs of different structures obtained via adjusting the thickness of Ag shells and tuning the molar ratio of Pd^{2+} ions to Ag atoms.

<table>
<tr><th>Molar ratio of Pd^{2+} to Ag(x)
Thickness of Ag shell (t)</th><th>0<x≤0.2</th><th>0.2<x≤0.3</th><th>0.3<x≤0.5</th><th>0.5<x<1</th></tr>
<tr><td>0< t < 3 nm</td><td colspan="4">CS Au@AgPd NPs</td></tr>
<tr><td>3 nm < t < 6 nm</td><td>Half-encased, CS Au@AgPd NPs</td><td colspan="2">Mixture of half-encased, CS Au@AgPd NPs and open-mouthed, YS Au@AgPd NPs</td><td>Open-mouthed, YS Au@AgPd NPs</td></tr>
<tr><td>t > 6 nm</td><td colspan="2">Half-encased CS Au@AgPd NPs</td><td colspan="2">Conventional YS Au@AgPd NPs</td></tr>
</table>

Table S3. Summary of absorption peak positions of Au cores and Ag shells from CS_n Au@Ag NPs with different thickness of Ag shells.

CS_n Au@Ag NPs	Thickness of Ag shell (nm)	Absorption peak position of Au cores (nm)	Absorption peak position of Ag shells (nm)
a	0	521	None
b	1.8±0.2	514	361
c	3.6±0.3	512	388
d	5.4±0.2	509	403
e	6.3±0.3	503	407
f	7.6±0.5	501	420

Table S4. The calculated refractive index of different solvents and the corresponding peak position of Au cores in the conventional (a) and open-mouthed, YS Au@AgPd NPs (b) in the different solvents.

Solvents	water	ethanol	THF	chloroform	toluene
N_{eff}	1.333	1.3614	1.4072	1.43736	1.60269
Peak position [a]	511.0	512.0	524.0	522.0	524.0
Peak position [b]	519.0	520.9	524.1	526.0	530.0

Table S5. Summary of ECSAs, potential values of oxidation peak, and current density normalized by Pd mass of GCE modified by open-mouthed, YS $Au_{0.70}@Ag_{0.17}Pd_{0.13}$ NPs, open-mouthed, hollow $Ag_{0.73}Pd_{0.27}$ NPs, conventional YS $Au_{0.42}@Ag_{0.33}Pd_{0.25}$ NPs,Hollow $Ag_{0.78}Pd_{0.22}$ NPs, CS $Au_{0.83}@Pd_{0.17}$ NPs and commercial Pd/C catalyst in 0.3 M N_2-saturated KOH aqueous solution at room temperature with a scan rate of 50 mV s^{-1}, respectively.

Samples	ECSA [$m^2\ g^{-1}$]	E [V]	Current density by mass normalization(Pd) [mA mg_{Pd}^{-1}]
Open-mouthed, YS $Au_{0.70}@Ag_{0.17}Pd_{0.13}$ NPs	87.8	-0.362	215.1
Open-mouthed, hollow $Ag_{0.73}Pd_{0.27}$ NPs	49.0	-0.341	128.3
Conventional YS $Au_{0.42}@Ag_{0.33}Pd_{0.25}$ NPs	49.6	-0.349	130.9
Hollow $Ag_{0.78}Pd_{0.22}$ NPs	51.6	-0.337	141.8
CS $Au_{0.83}@Pd_{0.17}$ NPs	29.5	-0.315	57.5
Pd/C catalyst	30.4	-0.369	119.8

The ECSAs of open-mouthed, YS Au@AgPd NPs, conventional YS Au@AgPd NPs and commercial Pd/C catalyst were estimated by the following equation, respectively:

$$ECSA = Q_0/q_0 \quad (3)$$

where Q_o is the surface charge that can be obtained via integrating from the area under the CV trace of oxygen desorption (-0.5 ~ -0.2 V), and q_o is the charge required for desorption of monolayer of oxygen on the Ag-Pd surface (430 μC/cm^2).

References

[1] H. B. Xia,S. Bai, J.Hartmann andD. Wang, *Langmuir* 2010, **26**, 3585-3589.

[2]H. Li, H. Xia,D. Wang and X. Tao, *Langmuir*2013, **29**, 5074-5079.

[3] E.González, J.Arbiol andV. F.Puntes, *Science* 2011, **334**, 1377-1380.

[4] G. Guisbiers andL.Buchaillot,*Nanotechnology* 2008, **19**, 435701-435705.

[5] D.Das, P. P. Chatterjee, I.Manna andS. K.A. Pabi,*Scr. Mater.*1999, **41**, 861-866.

[6] T. Shibata, B. A. Bunker, Z. Zhang, D. Meisel, C. F. Vardeman andJ. D. Gezelter,*J. Am. Chem. Soc.*2002, **124**, 11989-11996.

[7] L.Tang, B. C.Han, K.Persson, C.Friesen, T.He, K.Sieradzki andG.Ceder, *J.Electrochem. Soc.*2009, **132**, 596-600.

[8] E. F. Holby, W. C. Sheng, Y.Shao-Horn, D.Morgan,*Energy Environ. Sci.*2009,**2**, 865-871.

[9] D.Seo andH.Song,*J. Am. Chem. Soc*. 2009, **131**, 18210-18211.

[10] Z.Borkowska, A.Tymosiak-Zielinska andG.Shul, *Electrochim. Acta,* 2004, 49, 1209-1220.

[11] A.Hamelin, M. J.Sottmayor, F.Silva, S.-C. Chang andM. J.Weaver, *J. Electroanal. Chem.* 1990, **295**, 291-300.